ADVANCES IN ATMOSPHERIC SCIENCES, VOL. 40, JULY 2023, 1225–1243

• **Original Paper** •

Impact of Revised Trigger and Closure of the Double-Plume Convective Parameterization on Precipitation Simulations over East Asia

Xiaohan LI[1,2], Yi ZHANG[1,2], Yanluan LIN[3], Xindong PENG[*1,4], Baiquan ZHOU[1], Panmao ZHAI[1], and Jian LI[1]

[1]*State Key Laboratory of Severe Weather*, *Chinese Academy of Meteorological Sciences*, *Beijing* 100081, *China*

[2]2035 *Future Laboratory*, *PIESAT Information Technology Co Ltd.*, *Beijing* 100195, *China*

[3]*Department of Earth System Science*, *Ministry of Education Key Laboratory for Earth System Modeling*, *Institute for Global Change Studies*, *Tsinghua University*, *Beijing* 100084, *China*

[4]*CMA Earth System modeling and Prediction Center*, *Beijing* 100081, *China*

(Received 16 August 2022; revised 25 November 2022; accepted 16 December 2022)

ABSTRACT

A double-plume convective parameterization scheme is revised to improve the precipitation simulation of a global model (Global-to-Regional Integrated Forecast System; GRIST). The improvement is achieved by considering the effects of large-scale dynamic processes on the trigger of deep convection. The closure, based on dynamic CAPE, is improved accordingly to allow other processes to consume CAPE under the more restricted convective trigger condition. The revised convective parameterization is evaluated with a variable-resolution model setup (110–35 km, refined over East Asia). The Atmospheric Model Intercomparison Project (AMIP) simulations demonstrate that the revised convective parameterization substantially delays the daytime precipitation peaks over most land areas, leading to an improved simulated diurnal cycle, evidenced by delayed and less frequent afternoon precipitation. Meanwhile, changes to the threshold of the trigger function yield a small impact on the diurnal amplitude of precipitation because of the consistent setting of dCAPE-based trigger and closure. The simulated mean precipitation remains reasonable, with some improvements evident along the southern slopes of the Tibetan Plateau. The revised scheme increases convective precipitation at the lower levels of the windward slope and reduces the large-scale precipitation over the upper slope, ultimately shifting the rainfall peak southward, which is in better agreement with the observations.

Key words: convective parameterization, diurnal cycle of precipitation, East Asia, variable-resolution modeling

Citation: Li, X. H., Y. Zhang, Y. L. Lin, X. D. Peng, B. Q. Zhou, P. M. Zhai, and J. Li, 2023: Impact of revised trigger and closure of the double-plume convective parameterization on precipitation simulations over East Asia. *Adv. Atmos. Sci.*, **40**(7), 1225−1243, https://doi.org/10.1007/s00376-022-2225-9.

Article Highlights:

- A double-plume convective parameterization is improved by adding the effects of large-scale dynamic processes on the trigger of deep convection.
- The revised trigger and closure of convection substantially improve the diurnal phase of precipitation and yield a small impact on the diurnal amplitude.

1. Introduction

Precipitation over East Asia helps to feed about one-quarter of the world's population. Thus, accurately predicting precipitation is crucial in helping to manage water resources and protecting socioeconomic interests and human life against precipitation-related natural hazards such as floods and droughts. As a powerful tool for climate modeling, contemporary general circulation (global climate) models (GCMs) generally cannot well simulate precipitation characteristics in terms of their frequency, intensity, and diurnal cycle (Flato et al., 2013; Eyring et al., 2021). Specifically, for precipitation over East Asia that is strongly influenced by the sharp land-sea thermal contrast and the complex terrain around the Tibetan Plateau, the problems of GCMs in reproducing its spatial pattern and temporal evolution have been widely reported (Li et al., 2015; Zhang and Chen, 2016; Lin et al., 2019; Xin et al., 2020). For instance, the wet biases of

* Corresponding author: Xindong PENG
Email: pengxd@cma.gov.cn

summer rainfall at the southern and eastern edges of the Tibetan Plateau are commonly found in current GCMs (Yu et al., 2015; Zhang and Chen, 2016; Lin et al., 2018). The summer rainbands associated with the monsoon systems, which comprise significant variability at various spatial and temporal scales, are also a challenge for GCMs (Ding and Chan, 2005; Yu et al., 2007; Huang et al., 2013; Xin et al., 2020).

An important reason for the inadequate precipitation simulation lies in the parameterizations of hydrological processes and their interactions with large-scale dynamic processes. For instance, many GCMs cannot well simulate the diurnal variation of summertime rainfall, showing diurnal phases of ~3 to 4 h earlier over land; furthermore, they are unable to capture the nocturnal peaks even with finer resolutions (Covey et al. 2016; Tang et al., 2021). Earlier studies highlighted that the failure in simulating the diurnal cycle of precipitation could be largely attributed to the parameterized convection, especially those triggered based on the Convective Available Potential Energy (CAPE). The parameterized convection was too tightly coupled to the low-level thermodynamic properties controlled by solar insolation, triggering moist convection too early and too frequently during the day (Xie and Zhang, 2000; Yuan et al., 2013; Muetzelfeldt et al., 2021). Many efforts have been made to improve the diurnal cycle of precipitation, e.g., adding constraints associated with large-scale dynamical processes (e.g., low-level moisture convergence) to the convective trigger in an effort to relax the strong coupling between convection and the solar diurnal cycle (Bechtold et al., 2004; Kain, 2004; Wu et al., 2019; Xie et al., 2019).

The Global-to-Regional Integrated Forecast System (GRIST) is a unified system for global weather and climate modeling (Wang et al., 2019; Zhang et al., 2019, 2020, 2021, 2022; Li et al., 2020, 2022; Liu et al., 2020; Zhou et al., 2020; Li and Zhang, 2022). Currently, GRIST has two major working modes for climate and weather modeling. In climate mode, a modified physics suite, originally taken from the Community Atmosphere Model, version 5.3 (CAM5.3), was established and evaluated, with its convective parameterization replaced by a double-plume scheme (Li et al., 2022). In contrast to the separate representation of deep and shallow convection in CAM5 (Park et al., 2014), the double-plume scheme adopts a quasi-unified representation of shallow and deep convection within a single framework (Chu et al., 2022). This model was evaluated with a uniform resolution configuration (120 km) and was further subjected to a Variable-Resolution (VR) simulation with refinement over East Asia (110–35 km). Results demonstrated that the double-plume scheme reduced the biases of mean precipitation over the Indian Ocean and improved the representation of tropical variability. However, the premature peak of simulated precipitation over land, which occurs too early during the day, reveals its deficiency in capturing the diurnal cycle of rainfall. In the VR configuration, the wet biases of summer rainfall over the West Pacific and East Asia are reduced due to the refined grid spacing and terrain, but the inadequate diurnal cycle of precipitation persists across both the coarse- and fine-resolution versions of the model (Appendix A).

Xie and Zhang (2000) and Zhang (2002) proposed a convective quasi-equilibrium assumption that links convection to the dynamic CAPE generation rate by large-scale processes (referred to as dCAPE). In-depth analysis based on a single-column model test reveals high skill of dCAPE trigger regarding the ability to capture various convective systems over the Amazon region (Song and Zhang, 2017). Xie et al. (2019) applied the dCAPE trigger to the Zhang–McFarlane convective parameterization (Zhang and McFarlane, 1995) and also allowed moist convection to trigger below 600 hPa instead of in the planetary boundary layer (PBL). They showed considerable improvements in simulating the diurnal phase of precipitation at a 1° resolution, especially in capturing the eastward propagating signal over the United States. However, the diurnal amplitude of precipitation was weakened since the time for CAPE to reach its maximum during the day (i.e., CAPE-based closure) was often mismatched with the dCAPE trigger constrained by large-scale dynamic processes (Cui et al., 2021).

Motivated by Cui et al. (2021) and Xie et al. (2019), the effect of large-scale dynamic processes is added to the trigger of double-plume convection to improve the diurnal cycle of precipitation for GRIST. The closure is improved accordingly to avoid the potential reduction of the diurnal amplitude of precipitation. This study shows that the diurnal phase of precipitation is improved by considering the effect of large-scale dynamic processes on the initiation of deep convection. Meanwhile, changes in the threshold of the trigger function show a small impact on the diurnal amplitude of precipitation because of the consistent setting of the dCAPE-based trigger and closure.

The remainder of this paper is organized as follows. Section 2 briefly reviews the GRIST model and provides detailed information about the revision in the double-plume scheme. The experimental design and reference datasets are also given in section 2. Section 3 presents the evaluation of the simulated precipitation using the revised convective parameterization. Section 4 gives a summary and an additional discussion.

2. Model and experiment

2.1. *Model description*

The dynamical core of GRIST solves the primitive equations but has an option to restore the vertical acceleration term for nonhydrostatic modeling (Zhang et al., 2019, 2020). This layer-averaged, dry-mass, unstructured-mesh dynamical core allows both uniform-resolution and VR modeling within a unified global framework (Zhang et al., 2019; Zhou et al., 2020). It conserves a dry air mass to within machine accuracy and conserves the "total energy" within a magnitude that is suitable for global climate modeling.

The physics-dynamics coupling of GRIST supports the application of multiple physics suites (Zhang et al., 2020).

In this study, the hydrostatic core is coupled with a physics suite that was originally taken from CAM5.3. A pure operator-splitting approach is used for the physics-dynamics coupling (Li et al., 2022). It inherits several CAM5-derived parameterization schemes, including the UW moist PBL turbulence scheme (Bretherton and Park, 2009), the Morrison–Gettelman microphysics and Park macrophysics parameterizations (Gettelman et al., 2010; Park et al., 2014), and the RRTMG (Rapid Radiative Transfer Model for GCMs, Iacono et al., 2008). The convective parameterization uses a double-plume scheme (Chu et al., 2022; Li et al., 2022), with revisions in the trigger and closure of deep convection described in the next section. At the surface, the Noah-MP land model (Niu et al., 2011) is used. The fluxes over the ocean and sea ice use the formulation from CAM3 (Collins et al., 2004).

2.2. *The revised double-plume convective parameterization*

The default double-plume convective parameterization uses a pair of entraining/detraining plumes to describe deep and shallow convection independently. The plumes share the same buoyancy-sorting bulk mass flux cloud function but use different lateral mixing rates and trigger and closure assumptions. Entrainment occurs at the lateral boundary of the plume by turbulent mixing. The lateral mixing rate is set to a constant value of 3 km^{-1} for shallow convection. For deep convection, a mixing rate dependent on relative humidity is applied to inhibit deep convection in hostile environments (Chu et al., 2022). Detrainment includes the turbulent mixing at the lateral boundary, constrained detrainment at the top of a plume, and the effect of anisotropy that occurs at the level where the buoyancy starts to decrease with height. The precipitation formation and re-evaporation are calculated following Park and Bretherton (2009) but using different condensate threshold values (1 g kg^{-1} for deep convection and 0.5 g kg^{-1} for shallow convection).

Shallow convection is triggered if the turbulent kinetic energy (TKE) overcomes the convective inhibition (i.e., a CIN-TKE trigger). The trigger of deep convection is further determined by a dynamic CAPE production similar to that used in Wang and Randall (1994), i.e., deep convection is triggered when CAPE is generated at the previous time step, and sufficient TKE is present to overcome the CIN. The CAPE is calculated with a dilute plume approximation (Neale et al., 2008). Accordingly, a closure based on a dynamic CAPE quasi-equilibrium assumption is used for the deep plume, i.e., $\partial \mathrm{CAPE}/\partial t|_{\mathrm{L}} = \partial \mathrm{CAPE}/\partial t|_{\mathrm{cu}}$, assuming that the CAPE generated by non-convective processes (L) is balanced by the deep convective (cu) consumption (Zhang, 2002; Bechtold et al., 2014). The CAPE tendency due to convection is approximated by the heating through compensating environmental subsidence:

$$\left.\frac{\partial \mathrm{CAPE}}{\partial t}\right|_{\mathrm{cu}} = \frac{M_{\mathrm{b}}}{M_{\mathrm{b}}^{*}} \int_{z_{\mathrm{base}}}^{z_{\mathrm{top}}} \frac{g}{\overline{Tv}} \left(\frac{\partial \overline{Tv}}{\partial z} + \frac{g}{c_p} \right) M^{*} \mathrm{d}z \,, \qquad (1)$$

where M_{b} is the actual cloud base mass flux, M_{b}^{*} is a prescribed cloud base mass flux (set as 0.1 $m^2\ s^{-1}$), and M^{*} is the initial vertical mass flux profile obtained from the updraft computation based on M_{b}^{*}, $\overline{Tv}$ is grid-scale virtual temperature, and c_p is the specific heat at constant pressure. The cloud base mass flux is expressed as:

$$M_{\mathrm{b}} = M_{\mathrm{b}}^{*} \frac{\left.\dfrac{\mathrm{CAPE} - \mathrm{CAPE}'}{\Delta t}\right|_{\mathrm{L}}}{\displaystyle\int_{z_{\mathrm{base}}}^{z_{\mathrm{top}}} \frac{g}{\overline{Tv}} \left(\frac{\partial \overline{Tv}}{\partial z} + \frac{g}{c_p} \right) M^{*} \mathrm{d}z} \,, \qquad (2)$$

where the superscript $'$ denotes the atmospheric state after the calculation of the deep plume at the previous time step (regardless of whether it is triggered or not).

GRIST can produce an overall reasonable mean climate of circulation, precipitation, and radiation budget using this physics suite (Li et al., 2022). However, the peak of daytime precipitation occurs too early over land, thus revealing its deficiency in capturing the diurnal cycle of precipitation (cf., Fig. 8). We speculate that the initiation of deep convection is overly coupled to the solar diurnal cycle if solar radiation, surface heating, and PBL turbulence are considered to contribute to the onset of convection. Following Xie et al. (2019), the trigger of deep convection can be revised so that convection occurs only when the large-scale advection makes a positive contribution to the existing positive CAPE and the TKE overcomes the CIN. The threshold value for CAPE production by the dynamical core is 0 J kg^{-1} h^{-1} (denoted as dCAPE0). Cui et al. (2021) investigated the sensitivity of the dCAPE trigger to its threshold value (denoted as dCAPE*N*, $N > 0$ J kg^{-1} h^{-1}) in CAM5. They suggested that the diurnal phase of rainfall over the land can be further improved by setting the dCAPE threshold value as ~55 J kg^{-1} h^{-1}, at the expense of degraded mean precipitation (especially over the ocean) and a reduction in the diurnal amplitude of precipitation. Considering that the purpose of dCAPE*N* trigger is to relax the overly strong coupling between deep convection and surface heating, dCAPE*N* is only used over the land in this study to avoid the potential degradation over the ocean.

The key to improving the closure to avoid potential reduction of the diurnal amplitude of precipitation is to re-quantify the CAPE production by the non-convective processes under the more restricted trigger condition, i.e., whether to update CAPE$'$ in Eq. (2) when deep convection does not trigger. Here, we allow other physical processes, especially the shallow convection, to consume CAPE, that is if the CAPE at the current (n) time step is less than CAPE$'$, then $\mathrm{CAPE}'(n+1) = \mathrm{CAPE}$ (Fig. 1). Otherwise, CAPE$'$ remains unchanged, which means that the generated CAPE will be accumulated and consumed by deep convection once the revised dCAPE trigger is satisfied. It potentially allows the model to capture the transition of convection from shallow to deep, which is an important element for the diurnal cycle of precipitation (Zhang and Klein, 2010; Rio et al., 2019).

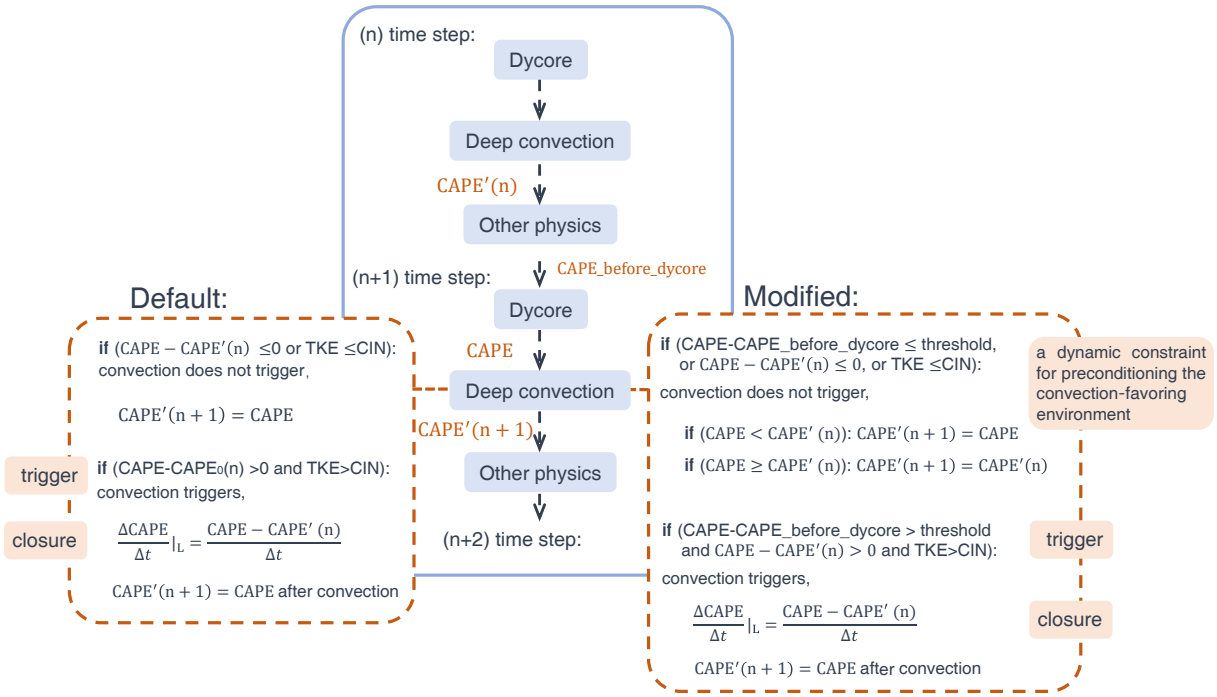

Fig. 1. Diagram showing the default and modified trigger and closure assumptions for the deep convection. Dycore refers to the dynamical core. The other physics processes contain the sequentially coupled cloud microphysics, radiation transfer, surface model, and PBL turbulence schemes.

The deep and shallow plumes are coupled in a parallel fashion and share the same cloud function, thus favoring the transition.

2.3. *Experiment design*

A VR model configuration (110–35 km) is used in this study, within which the highest resolution cells cover a part of continental East Asia and the surrounding islands and seas (Fig. 2). The VR configuration is chosen to examine the revised convective parameterization for two reasons. First, earlier modeling tests suggested that the VR model reduces the wet biases of mean precipitation over the West Pacific and East Asia. Thus, we may further explore improvements in the diurnal cycle of precipitation based on this added value of higher resolution for mean precipitation. Second, the VR setup provides a more challenging environment as the modification in convective parameterization may introduce additional sensitivities to the transition region due to the continuous changes in mesh size.

A series of AMIP-type sensitivity simulations were conducted (Table 1). The simulations were initiated in May 2000 and continuously integrated for 5.5 years using the preprocessed sea surface temperature and sea-ice concentration data (Taylor et al., 2000). The model output for 2001–05 was used to assess its representation of mean state and precipitation variability. The vertical resolution consists of a 30-full-level Lorenz grid with a model top at 2.25 hPa. The model (physical) time step (dt) was set to 300 s, and the dynamical core is sub-cycled with dt = 100 s within each model time step. The simulation using the default trigger and closure assumption of deep convection is referred to as CTRL. The two sensitivity experiments, dCAPE0 and dCAPE60, use the revised dCAPE trigger and closure with dCAPE threshold values set to 0 and 60 J kg^{-1} h^{-1}, respectively.

The satellite-based observational and reanalysis precipitation datasets used in this study include the products from the Global Precipitation Climatology Project (GPCP, 1979–2010, Adler et al., 2018) and the monthly mean ERA5 reanalysis (2001–20, Hersbach et al., 2020). These datasets evaluate the global mean precipitation and its seasonal variation and the 30-min Integrated Multi-satellite Retrievals for Global Precipitation Measurement (GPM) (IMERG, 2001–05, Huffman et al., 2018), as well as the hourly ERA5 datasets are used for assessing the diurnal cycle. Five sub-regions over China are chosen for further evaluation of the variability of precipitation at various temporal scales (Fig. 2, black boxes). These include the Tibetan Plateau (28°–35°N, 103°–108°E), Western Plain (28°–35°N, 103–108°E), Southwest China (23°–27°N, 100°–105°E), Eastern Plain (28°–35°N, 112°–120°E), and South China (23°–27°N, 112°–118°E).

3. Results

3.1. *Mean precipitation and seasonal variation*

Figure 3 compares the annual and boreal summer (June–July–August) mean precipitation from the observation/reanalysis and each model. The spatial correlations and

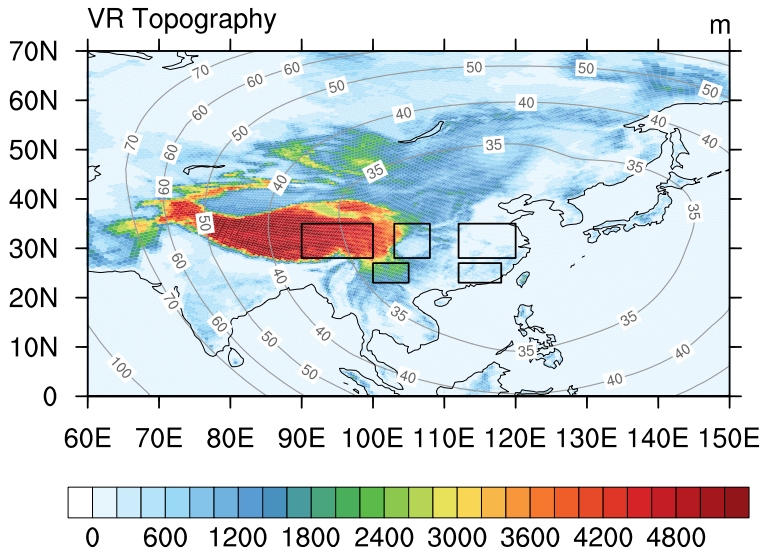

Fig. 2. Surface elevation over East Asia at 110–35 km resolution (units: m). The gray contours show the grid scales in VR modeling. The five rectangles correspond to the selected sub-regions over China for regional analysis: Tibetan Plateau (28°–35°N, 103°–108°E), Western Plain (28°–35°N, 103°–108°E), Southwest China (23°–27°N, 100°–105°E), Eastern Plain (28°–35°N, 112°–120°E), and South China (23°–27°N, 112°–118°E).

Table 1. Description of experiments.

Name	Resolution	Timestep	Trigger of deep convection	Closure of deep convection
CTRL	110–35 km, refined over East Asia	300 s	(1) Sufficient TKE to overcome the CIN; (2) CAPE is generated at the previous time step, $\left.\frac{\partial \mathrm{CAPE}}{\partial t}\right\|_{\mathrm{L}} \approx \left.\frac{\mathrm{CAPE}-\mathrm{CAPE}'}{\Delta t}\right\|_{\mathrm{L}} > 0$.	$\left.\frac{\partial \mathrm{CAPE}}{\partial t}\right\|_{\mathrm{L}} = -\left.\frac{\partial \mathrm{CAPE}}{\partial t}\right\|_{\mathrm{cu}}$, the dynamic CAPE is built up by all the non-convective processes at the previous step. The dynamic CAPE is represented by the net CAPE generation during the period that deep convection does not trigger.
dCAPE0	110–35 km	300 s	(1) Sufficient TKE to overcome the CIN; (2) CAPE is generated by dynamical core at the previous time step, i.e., dCAPE > 0 J kg^{-1} h^{-1}.	
dCAPE60	110–35 km	300 s	Same as dCAPE0, but increasing the threshold of CAPE production by dynamical core over the land, i.e., dCAPE > 60 J kg^{-1} h^{-1}.	Same as dCAPE0.

root-mean-square errors between the simulations and GPCP are given in the figure to quantify the model biases. The overall annual mean precipitation for CTRL resembles GPCP and ERA5, but it shows wet biases over the South Pacific Convergence Zone (SPCZ) and around the Maritime Continent. It has dry biases over South America and Southern Great Plains of the United States. In summer, the CTRL model overestimates precipitation over the Bay of Bengal, the Arabian Sea, the Maritime Continent, and the southern slopes of the Tibetan Plateau. Dry biases are found over the coastal areas of southeast China and the Sea of Japan.

The revised trigger and closure of deep convection primarily has an impact on the tropical precipitation (Figs. 3g–j). It reduces the wet biases over the Bay of Bengal, the Arabian Sea, and the Maritime Continent (located in the transition zone), and precipitation increases are found over the tropical Africa and the Amazon basins. In addition, the dry biases in summer rainfall over South China and the "Philippines hotspot" are reduced in the dCAPE0 and dCAPE60 models. Varying the threshold value of the convective trigger does not clearly impact the mean precipitation. The spatial pattern illustrating the precipitation discrepancy between dCAPE60 and CTRL is consistent overall with that between dCAPE0 and CTRL. The dCAPE0 model has slightly lower root-mean-square errors and higher spatial correlation coefficient than dCAPE60.

It is found that the CTRL model overestimates the summertime rainfall over the southern slope of the Tibetan Plateau, and the peak location is more northward than observed (Fig. 4a). This bias is more noticeable in the uniform 120 km resolution model (Fig. A1). It is attributed to the strong positive feedback between the large-scale condensation and the moisture convergence due to steep topography. Zhang and Li (2016) indicated that moisture convergence plays an important role in regulating the precipitation amount over the southern slopes of the Tibetan Plateau.

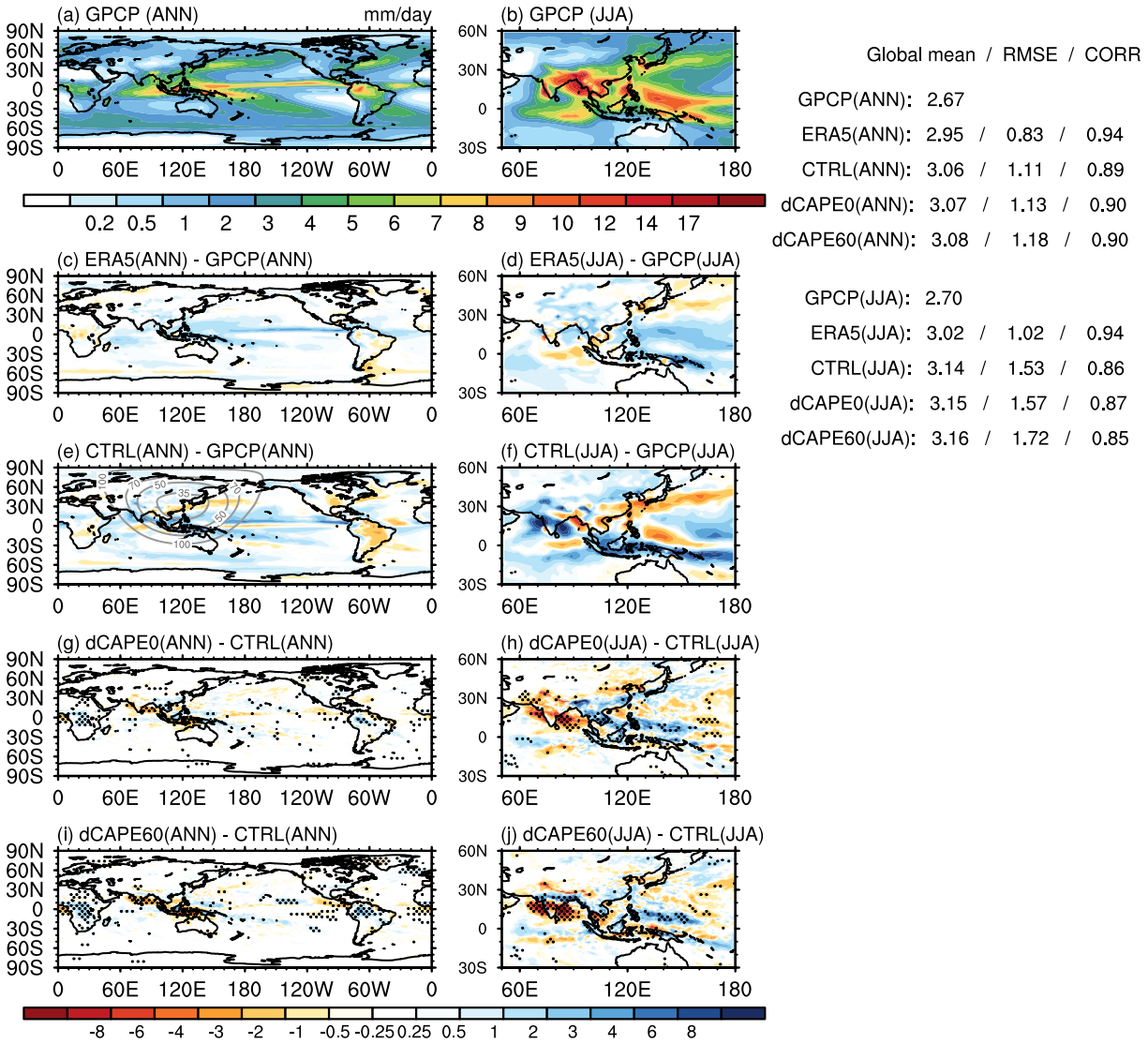

Fig. 3. (a) The annual (ANN) mean and (b) June–July–August (JJA) mean GPCP precipitation (units: mm d^{-1}). (c and d) The difference between ERA5 and GPCP. (e and f) The bias of CTRL against GPCP and the differences between the sensitivity experiments and CTRL; (g and h) dCAPE0 – CTRL and (i and j) dCAPE60 – CTRL. The gray contours in (e) show the grid scales in VR modeling. The stippled areas in (g)–(j) indicate that the difference between the sensitivity experiments and CTRL is statistically significant at the 0.05 level. Shown in the top right is the global mean precipitation of GPCP, ERA5, and each model, and the spatial correlations (CORR) and root-mean-square errors (RMSE) between the ERA5/modeled precipitation and GPCP.

Zhang et al. (2021) highlighted the importance of properly representing the condensation-advection processes on reducing the artificial rainfall peaks for GRIST over this region. In this model configuration, the wet bias in CTRL is partly corrected by the revised convective parameterization because of its impact on the moisture transport. The dCAPE0 and dCAPE60 models resemble the observed double-peak pattern of summer rainfall over this region; however, the modeled coastal peak is ~3° further north than the GPCP (Fig. 4a). They produce a greater amount of convective precipitation over the low levels of the windward slopes since the revised trigger of deep convection is linked to the large-scale dynamical processes such as low-level moisture convergence (Fig. 4b). The moisture transport process weakens, leading to a notable reduction in large-scale precipitation over the upper slope (Figs. 4d–f).

Figure 5 illustrates the zonally averaged precipitation amount and the convective-to-total precipitation ratio from the annual, summer, and winter (December–January–February, DJF) climatology. The zonally averaged annual mean total precipitation shows indiscernible changes, with the maximum in each model ~2 mm d^{-1} greater than that of GPCP. Differences are found in the partitioning of convective and large-scale precipitation among different configurations (Figs. 5d–f). The convective-to-total precipitation ratio in the observation is estimated to be around 50% in the tropics (Dai, 2006). The tropical and subtropical maximum convective precipitation fraction for GRIST is ~75% at 120 km reso-

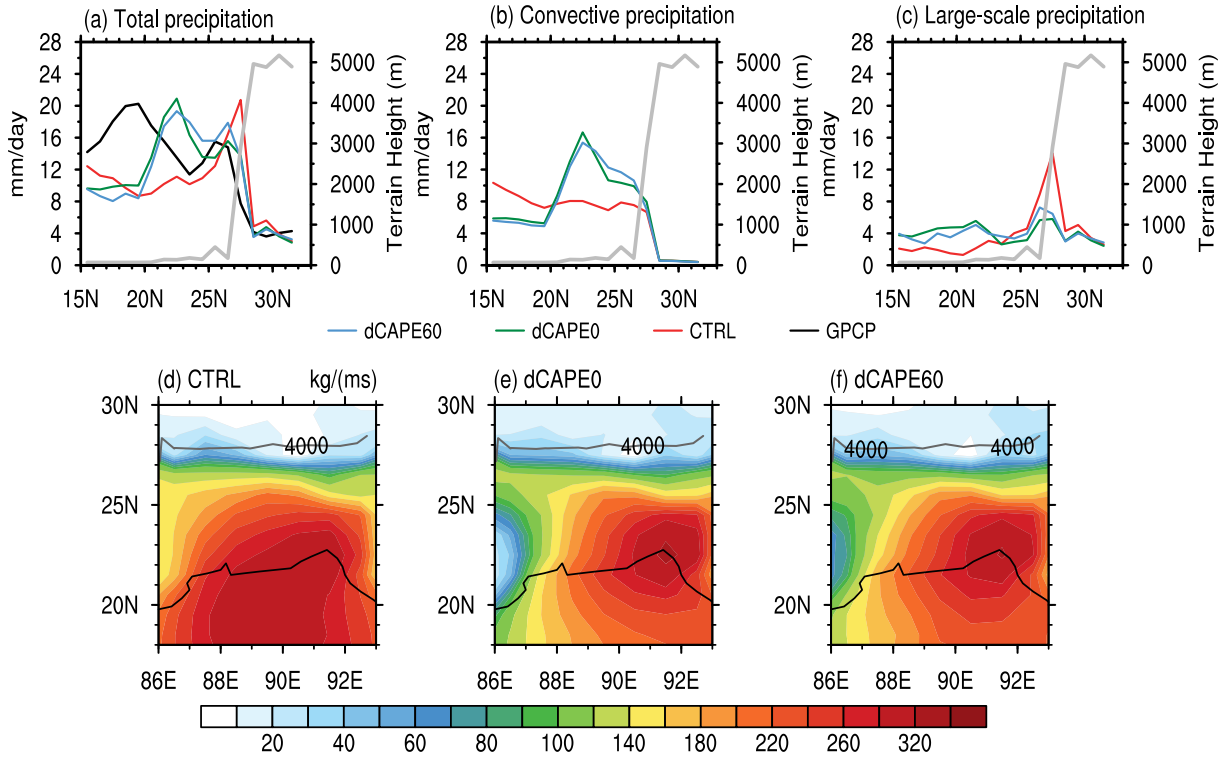

Fig. 4. (a) The meridional transects of precipitation zonally averaged along 86°–93°E in JJA (units: mm d^{-1}). Shown are GPCP (black), CTRL (red), dCAPE0 (green), and dCAPE60 (blue). The solid gray line shows the zonally averaged terrain height (units: m). (b) and (c) The same as for (a) but for the modeled convective and large-scale precipitation, respectively. (d)–(f) The v component of total column water vapor transport in JJA for (d) CTRL, (e) dCAPE0, and (f) dCAPE60. The gray curve represents a terrain height of 4000 m.

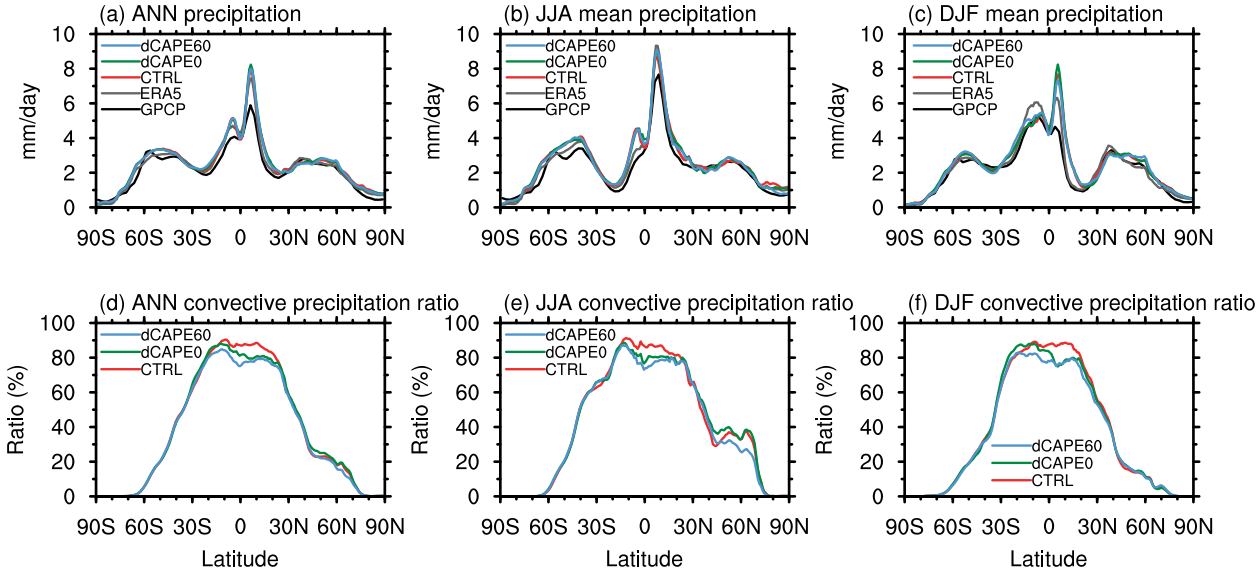

Fig. 5. Zonally averaged (a) annual mean precipitation for GPCP, ERA5, and each model (units: mm d^{-1}). (b) and (c) The same as for (a), but for the June–July–August (JJA) and December–January–February (DJF) mean, respectively. (d)–(f) The same as for (a)–(c), but for the model generated convective-to-total precipitation ratio.

lution (figure not shown). However, the VR CTRL model increases the convective-to-total precipitation ratio to ~90%, implying unrealistic, overly frequent precipitation events with extended durations but low intensity. This is primarily due to the smaller timestep used for the coarse mesh size in the VR modeling.

The overestimated ratio is reduced in the dCAPE0 and dCAPE60 models because a more restricted convective trigger acts to suppress weak convection. The convective-to-total precipitation ratio for dCAPE60 is about 80% in the trop-

ics. However, this ratio is still higher than the observed value and that of the 120-km simulation. To produce a more realistic precipitation partitioning in the GRIST-VR configuration, further improvements to physical parameterizations are necessary to correctly depict the interactions between subgrid scale convection and large-scale dynamic processes. For example, the stochastic method of Wang et al. (2018) notably reduced weak convective precipitation during the Indian summer monsoon, inspiring future improvements.

The summer monsoon plays a significant role in the seasonal variation of precipitation over Asia. Figs. 6a–e show the latitude and monthly migration of East Asian monsoon rainfall averaged for 110°–140°E. The pattern of precipitation migration for ERA5 is similar to GPCP, but the summertime rainfall amount is higher. The CTRL model reproduces the overall northward migration of rainband from May to July. But it underestimates the stationary mei-yu rain belt (around 32°N), and shifts the maximum center northward (see also Fig. 7). It also overestimates low-latitude precipitation during the retreat period of monsoon (from October to March). In contrast, the dCAPE0 and dCAPE60 models better capture the key features of rainfall variation. The underestimated mei-yu rain belt is ameliorated, and the maximum center is more consistently located with observations and reanalysis.

Over the South Asian monsoon region (Figs. 6f–j), the CTRL model overestimates precipitation over 10°–20°N from June to September. The dCAPE0 and dCAPE60 models move the maximum rainfall center northward in better agreement with the observations/reanalysis. They better capture the migrating rainfall feature associated with the onset and retreat of the South Asian monsoon. However, the maximum monsoon rainfall amounts near 22°N are still overestimated from June to September. Comparing dCAPE0 and dCAPE60, varying the threshold value of convection trigger over the land from 0 to 60 J kg^{-1} h^{-1} has a small overall impact on the seasonal variation of precipitation.

Figure 7 uses the differences of precipitation between June and May (and between July and June) to show the spatial pattern of rainfall variation corresponding to the summer monsoons. With the onset of the Indian summer monsoon, remarkable precipitation increases occur over the western coastal regions of the Arabian Peninsula and the Bay of Bengal as well as to the south of the Tibetan Plateau (Fig. 7a). The rainfall amounts over southeastern and southern China and Japan also increase due to the onset of the East Asian summer monsoon. The CTRL model reproduces the positive rainfall changes corresponding to the onset of Indian summer monsoon, but the increase in precipitation amount, especially over the Bay of Bengal, is larger than GPCP and ERA5. The dCAPE0 and dCAPE60 models ameliorate the overestimated precipitation over the southern portion of the Tibetan Plateau. They also better capture the spatial pattern of changes in rainfall associated with the onset of East Asian summer monsoon. From June to July, the CTRL model produces an artificial reduction of precipitation over the northwestern part of the Indochina Peninsula, which is largely corrected by dCAPE0 and dCAPE60. The dCAPE0 and dCAPE60 models reproduce the key features of rainfall variation between June and July, with positive (negative) changes that can be seen to the north (south) of 32°N, but they overestimate the increase of precipitation over northern India and the Bay of Bengal.

Figure 8 shows the annual precipitation cycles over the five sub-regions in China. The CTRL run produces the annual cycle consistent with GPCP and ERA5 over the Tibetan Plateau, the Western Plain, and South China. It pro-

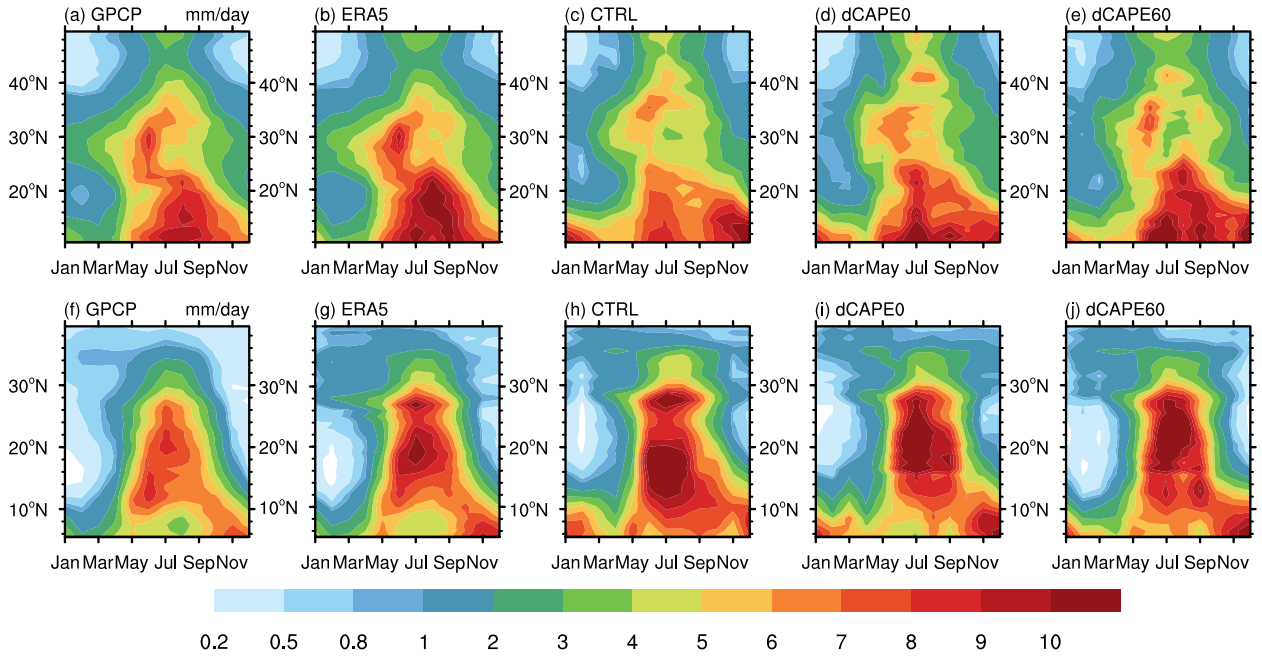

Fig. 6. Latitude-time variation of rainfall averaged for 110°–140°E (units: mm d^{-1}) from the (a) GPCP, (b) ERA5, and simulations for the (c) CTRL, (d) dCAPE0, and (e) dCAPE60. (f)–(j) The same as for (a)–(e) but averaged for 60°–105°E.

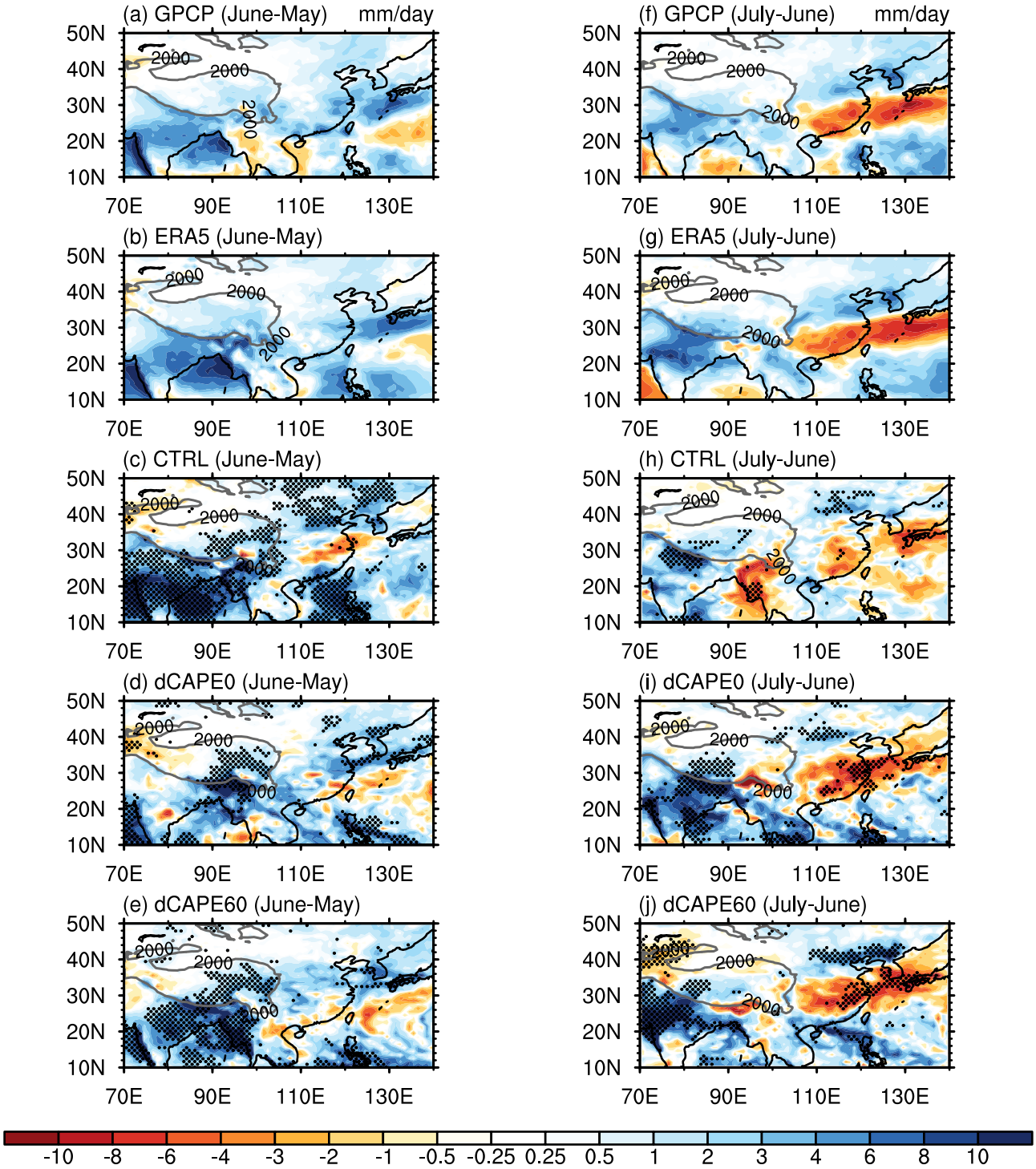

Fig. 7. Differences in precipitation amount (units: mm d^{-1}) between June and May (June minus May) from (a) GPCP, (b) ERA5, and simulations for (c) CTRL, (d) dCAPE0, and (e) dCAPE60. Black curves represent a terrain height of 2000 m. (f)–(j), same as for (a)–(e) but for the differences between July and June (July minus June). The stippled areas indicate that the difference is statistically significant at 0.05 level.

duces the peak timing about one month earlier than the GPCP and ERA5 over Southwest China and the Eastern Plain. The revised scheme impacts the annual cycle of precipitation over the Eastern Plain, Southwest China, and South China, as it tends to delay the rainfall peak time over these regions.

3.2. *Diurnal cycle of precipitation*

The aforementioned analysis suggests that the revised convective parameterization basically maintains the added

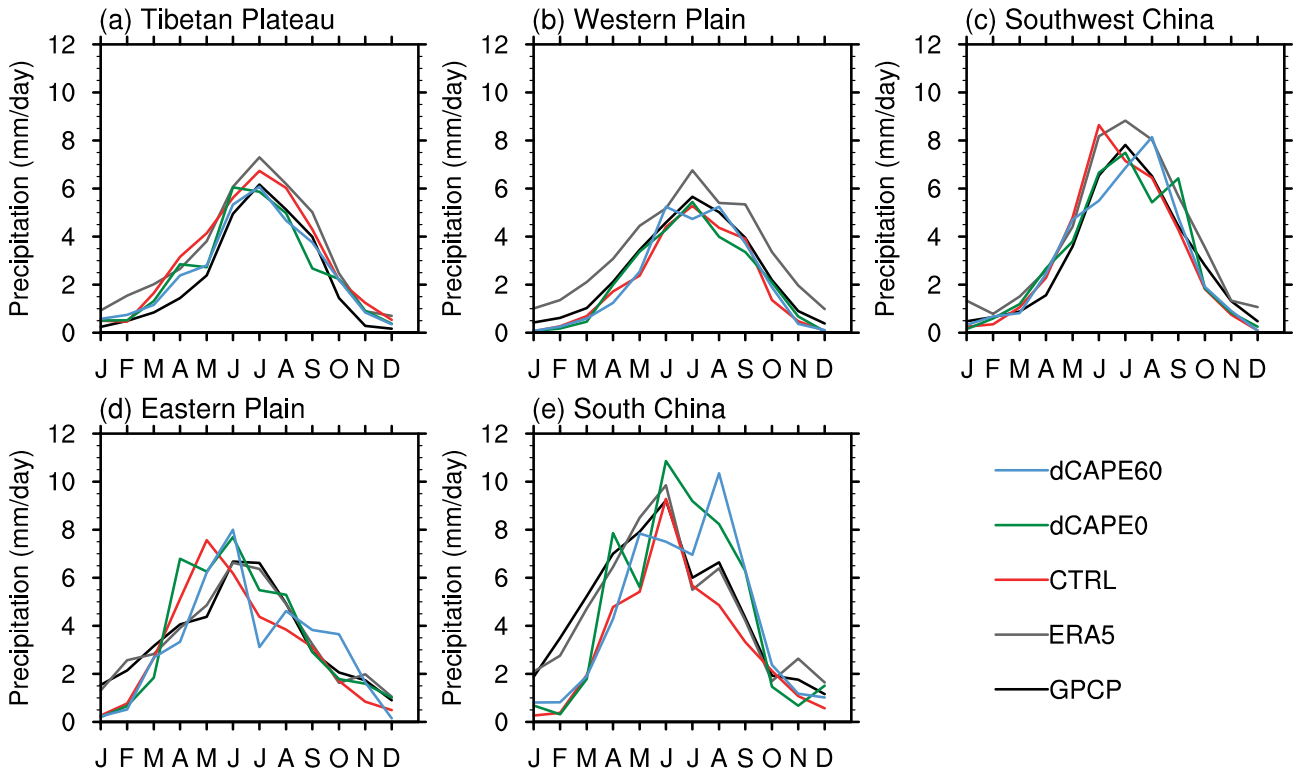

Fig. 8. Annual cycle of mean precipitation (units: mm d^{-1}) for GPCP, ERA5, and each model averaged over the five sub-regions denoted in Fig. 2: (a) Tibetan Plateau, (b) Western Plain, (c) Southwest China, (d) Eastern Plain, and (e) South China.

value of higher resolution for mean precipitation over East Asia. It also ameliorates the biases in the southern portion of the Tibetan Plateau, the Bay of Bengal, and the Arabian Sea. Varying the threshold value of the trigger function has a small overall impact on the mean precipitation and its seasonal variation. In addition to the mean state, the diurnal variation of precipitation is also an important aspect of evaluating how well the model reproduces the characteristics of precipitation.

The diurnal variation for boreal summer rainfall is evaluated with hourly model output using harmonic analysis (e.g., Dai, 2001). Figure 9 compares the modeled local solar time (LST) for the peaks of first harmonic cycle with GPM/ERA5. The observed maximum rainfall over land is location dependent and occurs most frequently in either late afternoon (1700 to 2200 LST) or from midnight to early morning (e.g., over the Tibetan Plateau and Sichuan Basin). The ERA5 tends to precipitate earlier than the GPM over major continents. The CTRL model peaks too early during the day (1200–1500 LST) and fails to capture the nocturnal peaks, except over the Tibetan Plateau, exhibiting common biases as shown in the lower-resolution version of GRIST (see also Fig. A2). Increasing the horizontal resolution over East Asia has an overall modest impact on improving the diurnal phase of precipitation, which is consistent with the VR simulations of the Energy Exascale Earth System Model Atmosphere Model version 1 that uses the Zhang–McFarlane parameterization (Tang et al., 2019).

It is found that the modeled diurnal cycle of precipitation by the default double-plume scheme is too tightly coupled to the solar diurnal cycle. This is because solar radiation, accompanied by surface heating and boundary layer turbulence, contributes to the initiation of deep convection during the day. After applying the revised dCAPE trigger and closure, a substantial delay in the rainfall peak over most land areas is seen, especially in the dCAPE60 model. The rainfall peak over India is delayed to ~1700 LST, and late afternoon to night rainfall peaks are found over Southwest and Northeast China. Over the United States, the dCAPE60 model captures the eastward propagating signal from downstream of the Rockies (late afternoon) to the adjacent Great Plains (nocturnal-to-early-morning), showing a model-independent feature of dCAPE trigger similar to that exhibited in Cui et al. (2021) and Xie et al. (2019) [Fig. S1 in the electronic supplementary material (ESM)]. The performance of dCAPE60 over tropical Africa is dependent on the location. Nevertheless, this approach shows promise in capturing some propagating signals and nocturnal peaks associated with mesoscale convective systems in this region (Yang and Slingo, 2001).

Cui et al. (2021) and Xie et al. (2019) indicated that using a dCAPE trigger in the Zhang–McFarlane parameterization (with a CAPE-based closure) leads to a substantially weaker diurnal amplitude of precipitation than observations because of the time needed for increased CAPE to reach its maximum during the day is mismatched with the dCAPE trigger constrained by large-scale dynamic processes (cf., Fig. 2 in Cui et al. (2021)). The weakened diurnal amplitude of precipitation is largely corrected by a consistent setting of

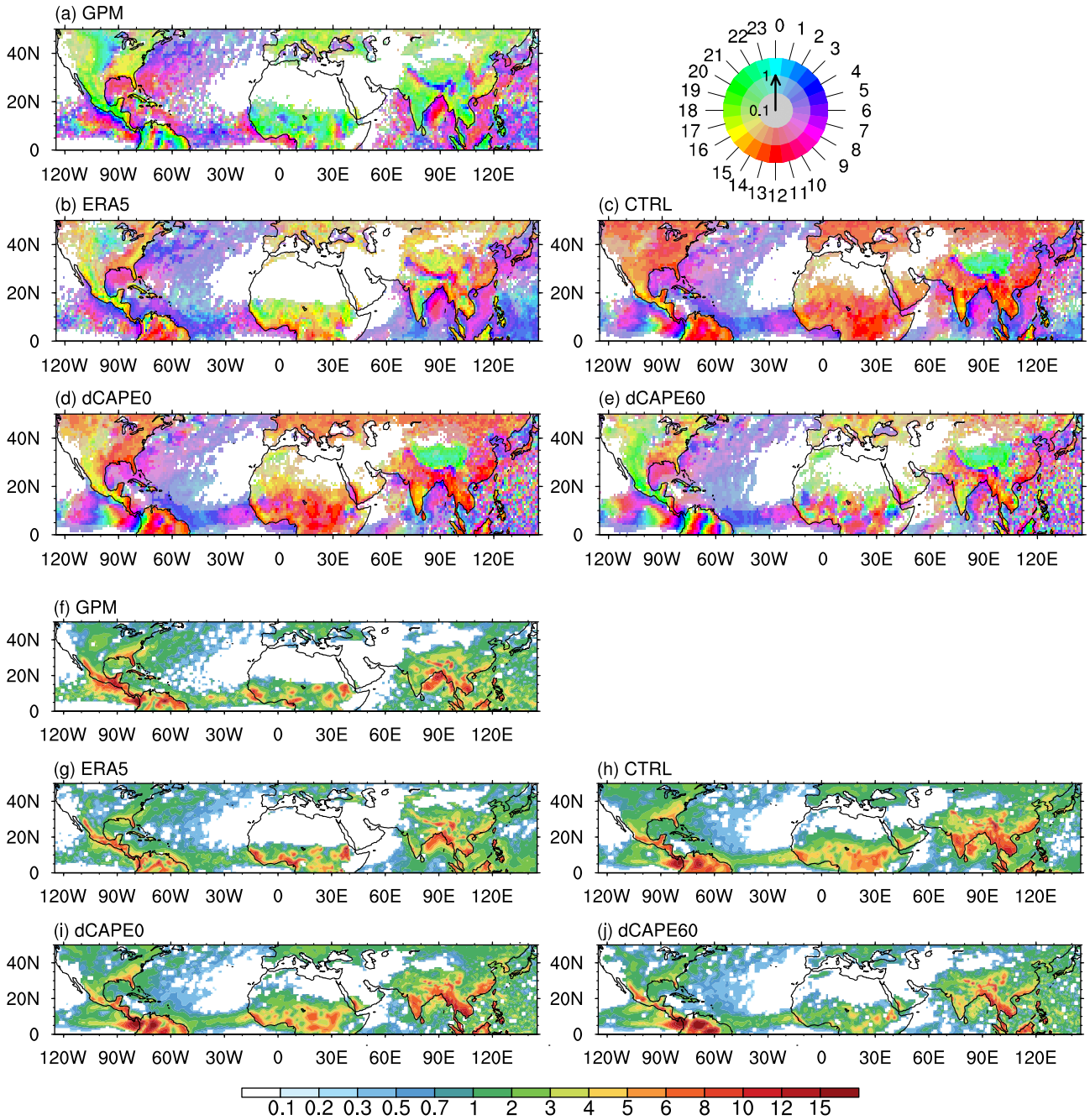

Fig. 9. Diurnal peak time (LST) of the first harmonic of precipitation during JJA for (a) GPM, (b) ERA5, (c) CTRL, (d) dCAPE0, and (e) dCAPE60. The 24-h phase dial is given in the top right, with the phase (local time) of the maximum indicated by colors, while the magnitude is indicated by the color saturation. (f)–(j) Same as for (a)–(e), but shows the diurnal amplitude of the precipitation (units: mm d^{-1}) for the GPM, ERA5, and each model.

dCAPE-based trigger and closure for deep convection (Figs. 9f–j). Consequently, all models reproduce the observed diurnal amplitude of precipitation. Over East Asia, dCAPE60 produces a spatial pattern of diurnal amplitude that is close to that of the GPM.

Figure 10 shows the normalized diurnal cycle (by daily means) of precipitation amount, frequency, and intensity over the selected sub-regions. The precipitation amount, frequency, and intensity are calculated following Chen and Dai (2018). Generally, a more restricted convective trigger delays and reduces the precipitation frequency in the afternoon. The diurnal amplitude of precipitation intensity is also reduced over Southwest China and the Eastern and Western Plain.

Over the main body of the Tibetan Plateau, the observation shows a late afternoon peak (around 1800 LST) in precipitation amount and frequency. Chen et al. (2012) indicated that the rainfall peak from rain gauge observations has a later shift of ~3 h because the rain gauges capture rainfall in the valleys while satellites capture it over the mountains.

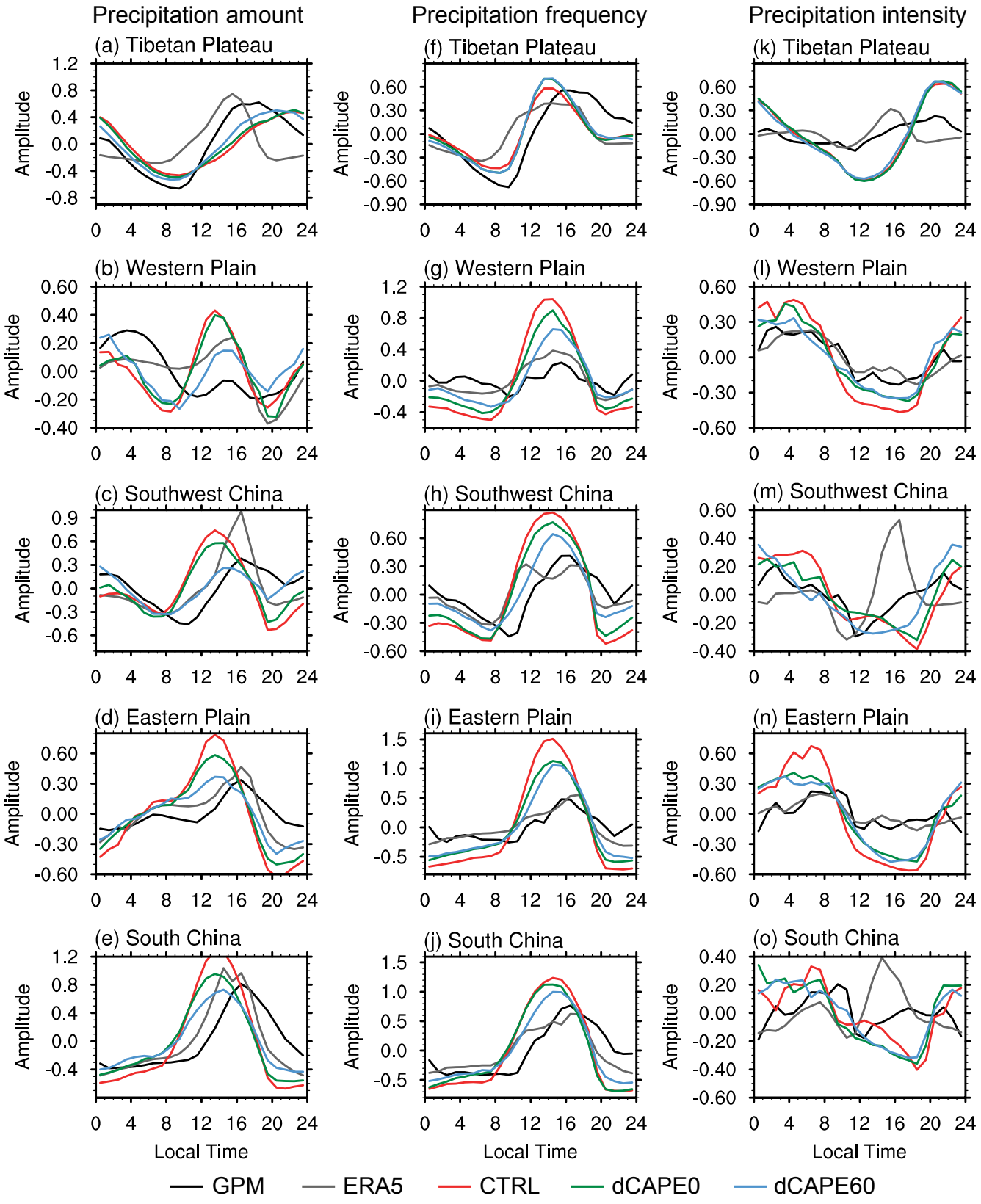

Fig. 10. Normalized (by daily mean) mean diurnal cycle of summer precipitation (a)–(e) amounts, (f)–(j) frequency, and (k)–(o) intensity averaged over the five sub-regions denoted in Fig. 2. Shown are GPM (black), ERA5 (gray), and modeling results from CTRL (red), dCAPE0 (green), and dCAPE60 (blue). The amount is defined as the accumulated precipitation over a given period, the frequency is defined as the percentage of the hours that have measurable precipitation (>0.1 mm d^{-1}) during the period, and the intensity is defined as the average precipitation rate over the precipitating hours.

The nighttime rainfall is barely captured by ERA5, indicating a rainfall peak at around 1600 LST. In contrast, all models perform reasonably well in reproducing the diurnal phase of precipitation amount and intensity over the Tibetan Plateau. The simulated diurnal amplitude in precipitation intensity is stronger than the satellite observation.

The Western Plain is dominated by early-morning rainfall, clearly seen in the diurnal cycle of observed precipitation amount and intensity. The CTRL model has a spurious rainfall peak in the afternoon with high frequency and low intensity. It reproduces the early-morning peak but has an earlier shift of ~2 hours. The dCAPE60 model substantially reduces the spurious instability-related (convective) precipitation by suppressing the precipitation frequency in the afternoon. The early-morning peak over this region is therefore highlighted. However, the revised dCAPE trigger and closure seem to have a limited ability to delay the early-morning rainfall peak, with an earlier shift still shown in both dCAPE0 and dCAPE60. One possible reason is that the convective parameterization cannot reasonably describe organized convection over this region (Rio et al., 2019; Chen et al., 2021). The eastward propagating large-scale precipitation does not dominate total precipitation over this region (see also Fig. 11). Therefore, the model cannot capture the eastward propagating convective systems.

A double-peak feature is observed over Southwest China. One peak occurs in the late afternoon (around 1700 LST) with high frequency and low intensity, and the other

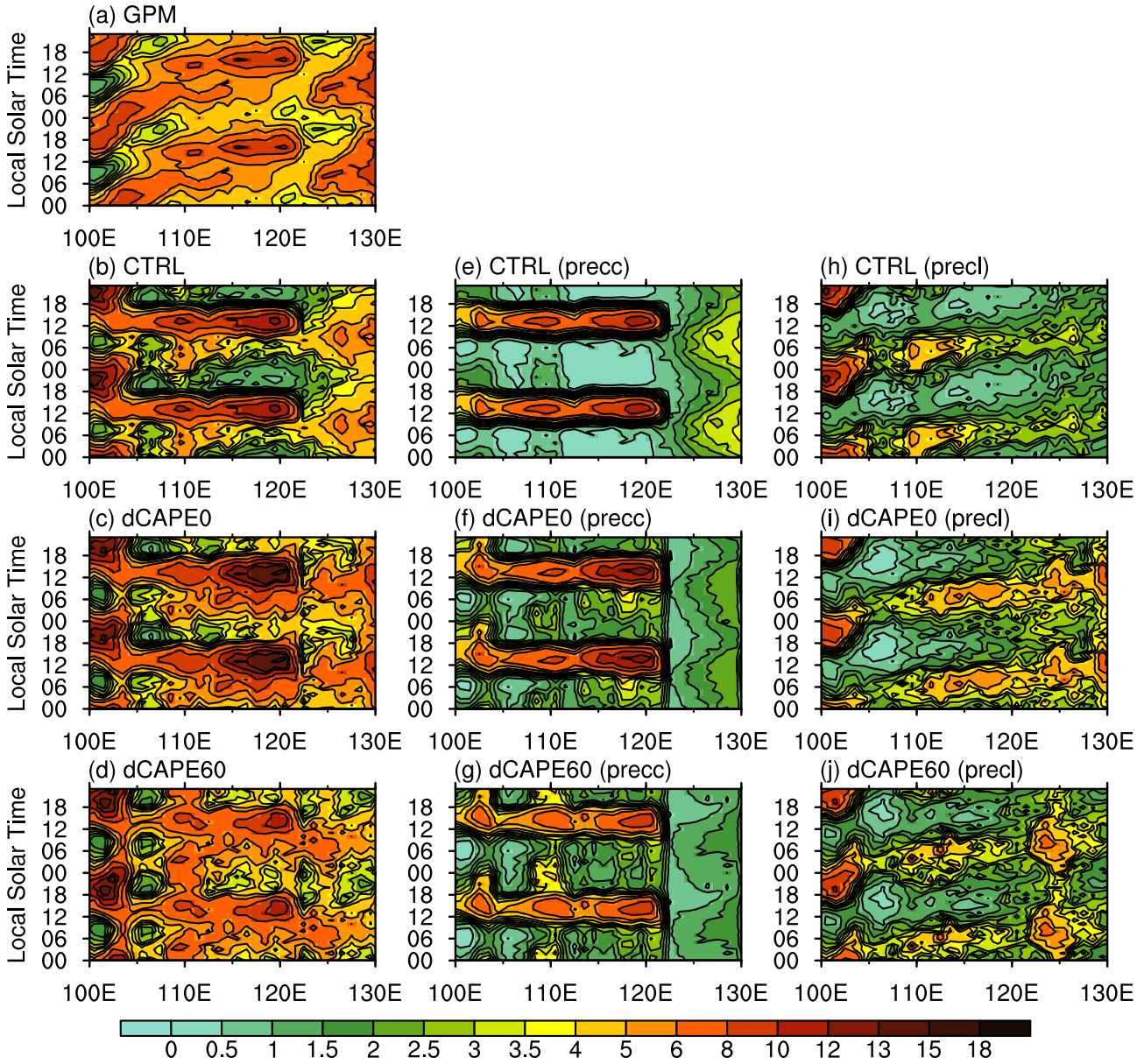

Fig. 11. Hovmöller diagram of hourly rainfall in JJA averaged over the area bounded by 27°–32°N and 100°–130°E for the (a) GPM, (b) CTRL, (c) dCAPE0, and (d) dCAPE60 (units: mm d^{-1}). (e)–(g) and (h)–(j) Same as for (b)–(d) but for the convective precipitation (precc) and large-scale precipitation (precl), respectively.

occurs at midnight (around 0200 LST) with high intensity. The CTRL model underestimates the midnight peak. Conversely, it overestimates the afternoon peak and shifts it 5-h earlier. The biased diurnal cycle of precipitation frequency is the main contributing factor. The revised dCAPE trigger and closure increase the frequency of precipitation during nighttime and reduces and delays it in the afternoon, improving the diurnal precipitation cycle over this region. The diurnal variation of rainfall intensity also agrees better with the observation. Comparing dCAPE0 and dCAPE60, increasing the threshold value of the convection trigger enhances the impact on delaying and reducing the afternoon rainfall peak.

Over the Eastern Plain, the observed rainfall presents a dominant rainfall peak in the afternoon (around 1600 LST) and a secondary peak in the early morning (around 0600 LST). The CTRL model captures the double-peak feature, but it overestimates the afternoon rainfall peak and produces a 3-h earlier shift in the peak time. This overestimated afternoon peak is reduced and slightly delayed in dCAPE0 and dCAPE60. Yuan et al. (2013) reported that the double-peak feature of CAM5 in the mei-yu region is due to opposing phases regarding convective precipitation (peaks in the afternoon) and large-scale precipitation (peaks in the early morning). The revised dCAPE trigger and closure suppress and delay the (convective) precipitation frequency in the afternoon; consequently, simulations agree better with the observations.

South China is a typical warm-season climate regime dominated by instability-related late afternoon convection, which tends to peak at ~1600 LST (mainly indicated by the precipitation frequency). All the models exhibit the typical daytime convection development caused by surface heating, with rainfall peaks at ~1400 LST. The dCAPE60 reduces the diurnal variation of precipitation frequency and amounts, but it only exerts a small impact on delaying the peak time.

Over East Asia, a typical summer rain belt is the zonal domain extending from the eastern slope of the Tibetan Plateau to the Yangtze River valley, including the subtropical mei-yu front. Figure 11 shows a Hovmöller diagram of precipitation averaged for 27°–32°N. The regional features shown in observations include the eastward propagating rainfall from the lee side of the Tibetan Plateau, the co-existence of early morning and late afternoon peaks over central-eastern China, and the morning rainfall over the East China Sea. The CTRL run produces a nearly stationary (convective) precipitation center from the lee side of the Plateau into eastern China, where the maximum precipitation occurs in the early afternoon. In contrast, dCAPE60 reproduces most observed features except for a weaker propagating signal at 105°–108°E. The revised dCAPE trigger and closure improve the simulated diurnal cycle by reducing the convective precipitation in the afternoon, which, in turn, leads to more large-scale precipitation that exhibits an eastward propagating signal.

The weaker eastward propagation of precipitation over the Western Plain explains the underestimation of early-morning rainfall over this region. It implies that the parameterized convection does not have a close enough relationship with the resolved-scale model dynamics; thus, only the large-scale precipitation exhibits an eastward propagating signal. The simulated diurnal cycles of convective and large-scale precipitation are very similar to CAM5 (e.g., Yuan et al., 2013) but rather different from those shown in Zhang et al. (2021), in which GRIST uses a different physics suite. In Zhang et al. (2021), parameterized convection contributed to a clear eastward propagating signal downstream of the Tibetan Plateau. It exhibited a response to the large-scale dynamical forcing similar to grid-scale precipitation. It also played a dominant role in regulating the precipitation simulation. Since the dynamical core is shared, this difference suggests that physical processes, including, but not limited to, convective parameterization, are essential in representing the propagation of rainfall over East Asia. In particular, the response of model convection (either explicitly represented by the dynamics-microphysics interaction or implicitly represented by cumulus parameterization) to nocturnal moisture convergence downstream of the Tibetan Plateau is essential. Ongoing analysis has been carried out to analyze this issue further.

4. Conclusion and discussion

This study improves the diurnal cycle of precipitation simulation for GRIST by adding the large-scale dynamic constraints on the trigger of deep convection. The original double-plume scheme indicates a premature peak of precipitation during the day over land, revealing its deficiency in capturing the diurnal cycle of summer rainfall even at higher resolution. To improve the diurnal cycle of precipitation, an empirical dynamic restriction suggested by Xie and Zhang (2000) is added to the combined dCAPE and CIN-TKE trigger of deep convection. The closure assumption is revised accordingly to allow other processes to consume CAPE under the more restricted convective trigger condition. The revised convective scheme is assessed with a variable-resolution model setup, and its impact on the mean state and variability of precipitation is evaluated. The major conclusions are as follows.

The revised convective parameterization generally maintains the added value of higher resolution for mean precipitation over East Asia. It ameliorates the wet biases in summer rainfall over the Bay of Bengal and the Arabian Sea and better captures the key features of rainfall migration associated with the onset and retreat of the Asian monsoon. Varying the threshold value of the dCAPE trigger from 0 to 60 J kg^{-1} h^{-1} has an overall small impact on the global mean precipitation and its seasonal variation. In addition, improvements are seen in the summer mean precipitation over the southern slopes of the Tibetan Plateau. The revised scheme increases the convective precipitation at the lower levels of the windward slopes, thus weakening moisture transport and reducing the large-scale precipitation over the upper slopes. The

revised scheme shifts the peak southward, leading to a better agreement with the observations.

The diurnal precipitation cycle over land is substantially improved by applying the revised dCAPE trigger and closure of deep convection, especially by increasing the dCAPE trigger threshold to 60 J kg^{-1} h^{-1}. A notable delay of daytime rainfall peak is found over East Asia. The subsequent potential problem of dCAPE trigger that reduces the diurnal amplitude of precipitation, as indicated by Cui et al. (2021) and Xie et al. (2019), is avoided by the consistent setting of the dCAPE-based trigger and closure. Further analysis indicates that the dCAPE60 model improves the diurnal cycle of precipitation by delaying and reducing the afternoon peak in precipitation frequency, thus, highlighting the large-scale nighttime precipitation with a propagating feature. The overly strong coupling between the initiation of deep convection and the solar diurnal cycle is relaxed.

In addition to East Asia, improvements in the diurnal cycle of precipitation by the revised convective parameterization are found over areas such as the Southern Great Plains (SGP) of the United States. It captures the eastward propagating signal downstream of the Rockies in the late afternoon to the SGP at midnight, alleviating the problem of a premature daytime peak (Fig. S1 in the ESM), a result consistent with Cui et al. (2021) and Xie et al. (2019), which used different modeling systems. It demonstrates that a model-independent feature in the form of a dCAPE trigger improves the diurnal phase of precipitation. The revised closure of convection yields further improvements in the diurnal amplitude of precipitation and will also benefit other modeling systems that have difficulties in representing the diurnal cycle.

Acknowledgements. This study was supported by the National Key R&D Program of China on the Monitoring, Early Warning, and Prevention of Major Natural Disasters (Grant Nos. 2018YFC1507005 and 02017YFC1502202).

Data Availability Statement. The observational datasets used in this study are available from GPCP —https://www.esrl.noaa.gov/psd/data/gridded/data.gpcp.html; and GPM—https://doi.org/10.5067/GPM/IMERG/3B-HH/06. The model output data supporting this study are available in the open data repository Zenodo at: https://doi.org/10.5281/zenodo.6501705.

Electronic supplementary material: Supplementary material is available in the online version of this article at https://doi.org/10.1007/s00376-022-2225-9.

APPENDIX A

Intercomparison of the Precipitation Simulation at 120 km and 110–35 km Resolutions

This section compares the JJA mean precipitation and its diurnal variation simulated at a uniform 120 km resolution (G6_CTRL) and 110–35 km variable resolution (VR_CTRL). Figure A1 displays the bias of JJA mean precipitation against GPCP from G6_CTRL and the difference between VR_CTRL and G6_CTRL. G6_CTRL shows wet biases over the West Pacific (especially in the "Philippines hotspot") and around the Maritime Continent. Over East Asia, it overestimates summer rainfall over most land areas of China and shows overly excessive precipitation over the southern slopes of the Tibetan Plateau. Compared to G6_CRTL, the VR model decreases the artificial precipitation over the "Philippines hotspot" and East Asia. In addition, the rainfall peak over the southern slopes of the Tibetan Plateau is slightly shifted southward by VR_CTRL.

Figure A2 shows the modeled diurnal phase and diurnal amplitude of summer rainfall for G6_CTRL and VR_CTRL. G6_CTRL peaks too early during the day (1200–1500 LST) over the land and fails to capture the nocturnal peaks, except over the Tibetan Plateau. VR_CTRL shows a pattern of diurnal phase generally consistent with that in G6_CTRL. The diurnal amplitude over East Asia is slightly larger in the VR model than in G6_CTRL since more grid-scale precipitation is resolved at a higher resolution.

Figure A3 compares the Hovmöller diagram of precipitation between G6_CTRL and VR_CTRL over East Asia. Both models produce a nearly stationary convective precipitation center in the afternoon and an eastward-propagating area of large-scale precipitation. VR_CTRL increases both

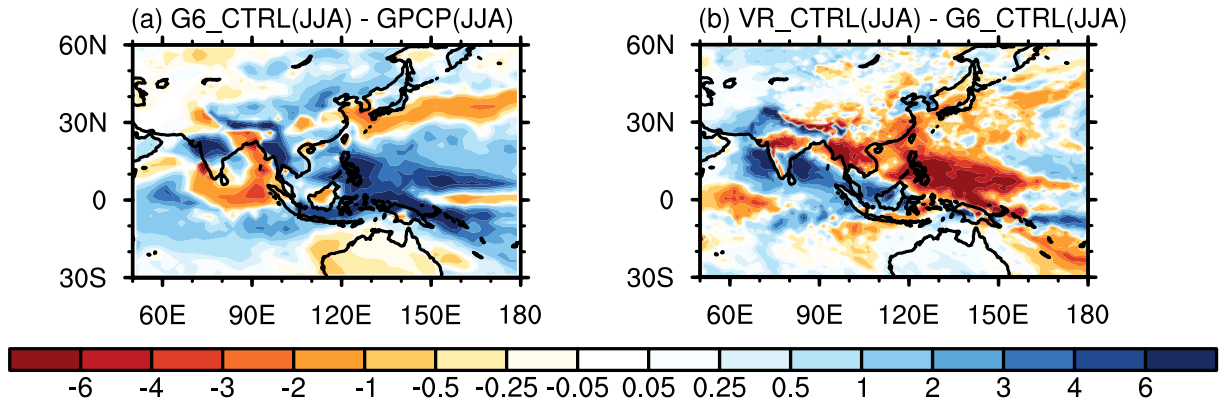

Fig. A1. (a) The bias of JJA mean precipitation against GPCP from G6_CTRL (units: mm d^{-1}), and (b) differences between VR_CTRL and G6_CTRL.

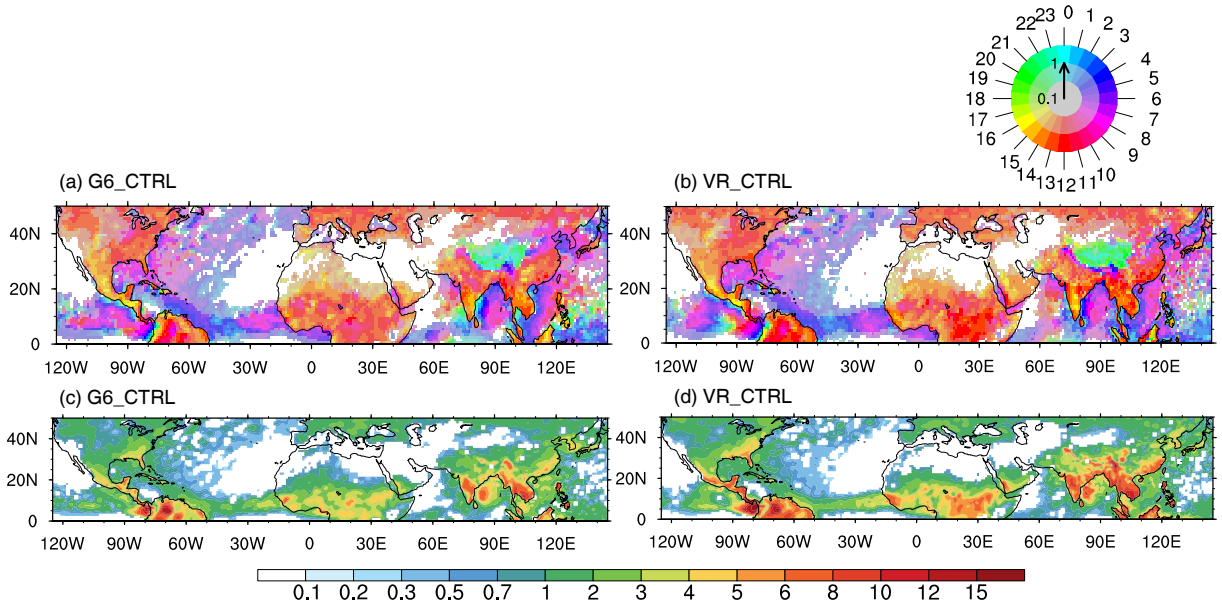

Fig. A2. Diurnal peak time (LST) of the first harmonic of precipitation during JJA for (a) G6_CTRL and (b) VR_CTRL. (c)–(d) Same as for (a)–(b) but show the diurnal amplitude of the precipitation (units: mm d^{-1}).

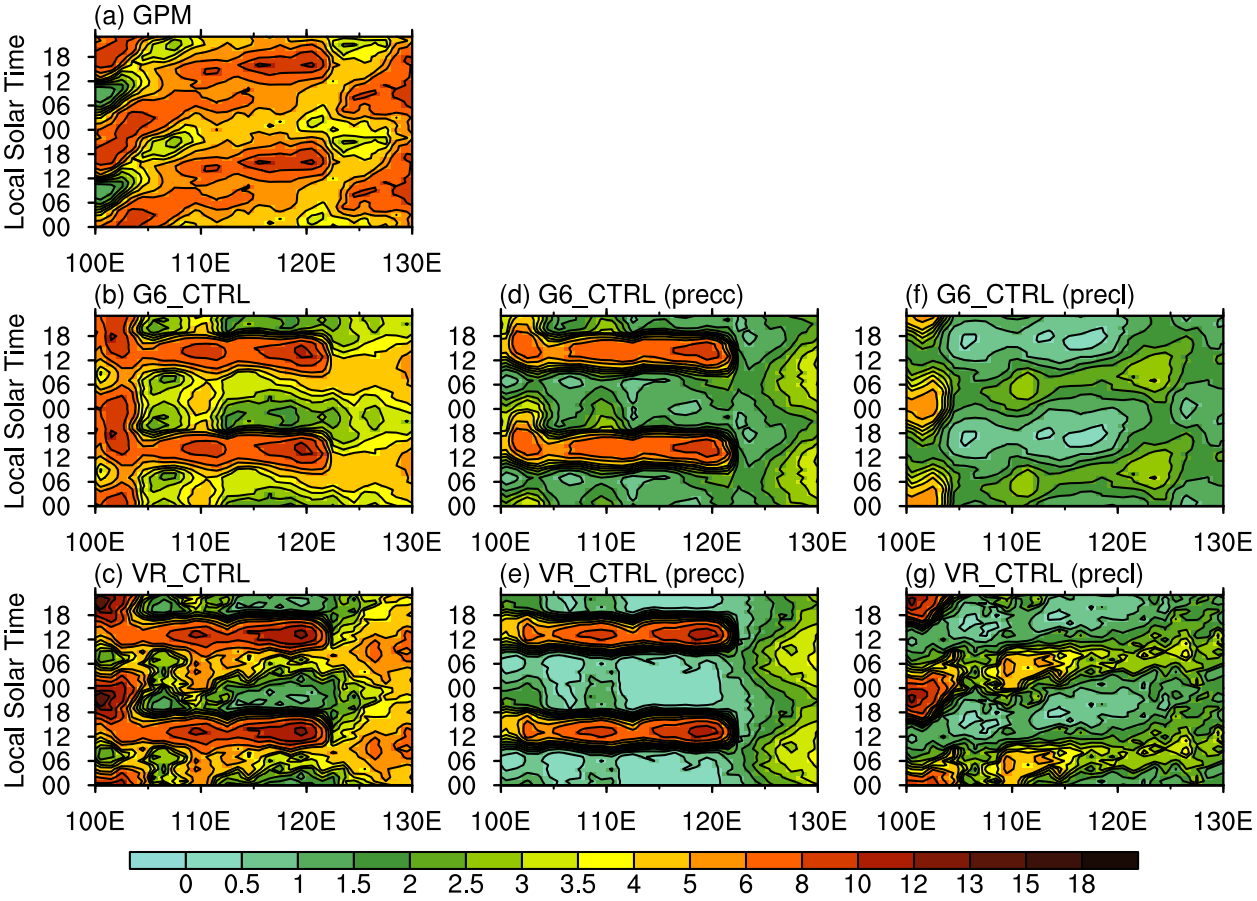

Fig. A3. Hovmöller diagram of hourly summertime rainfall averaged over the area bounded by 27°–32°N and 100°–130°E for (a) GPM, (b) G6_CTRL, and (c) VR_CTRL (units: mm d^{-1}). (d–e) and (f–g) Same as for (b and c) but for the convective precipitation (precc) and large-scale precipitation (precl), respectively.

the convective and large-scale precipitation, as compared with G6_CTRL. But the propagating pattern of precipitation is very similar between VR_CTRL and G6_CTRL. In summary, the VR model reduces some regional biases of mean

precipitation around East Asia. But the increased resolution (from 120 km to 35 km) and refined terrain have a limited impact on the diurnal cycle of precipitation.

REFERENCES

Adler, R. F., and Coauthors, 2018: The global precipitation climatology project (GPCP) monthly analysis (new version 2.3) and a review of 2017 global precipitation. *Atmosphere*, **9**, 138, https://doi.org/10.3390/atmos9040138.

Bechtold, P., J.-P. Chaboureau, A. Beljaars, A. K. Betts, M. Köhler, M. Miller, and J.-L. Redelsperger, 2004: The simulation of the diurnal cycle of convective precipitation over land in a global model. *Quart. J. Roy. Meteor. Soc.*, **130**, 3119–3137, https://doi.org/10.1256/qj.03.103.

Bechtold, P., N. Semane, P. Lopez, J.-P. Chaboureau, A. Beljaars, and N. Bormann, 2014: Representing equilibrium and nonequilibrium convection in large-scale models. *J. Atmos. Sci.*, **71**, 734–753, https://doi.org/10.1175/JAS-D-13-0163.1.

Bretherton, C. S., and S. Park, 2009: A new moist turbulence parameterization in the community atmosphere model. *J. Climate*, **22**, 3422–3448, https://doi.org/10.1175/2008JCLI2556.1.

Chen, C.-C., J. H. Richter, C. Liu, M. W. Moncrieff, Q. Tang, W. Lin, S. Xie, and P. J. Rasch, 2021: Effects of organized convection parameterization on the MJO and precipitation in E3SMv1. Part I: Mesoscale heating. *Journal of Advances in Modeling Earth Systems*, **13**, e2020MS002401, https://doi.org/10.1029/2020MS002401.

Chen, D., and A. G. Dai, 2018: Dependence of estimated precipitation frequency and intensity on data resolution. *Climate Dyn.*, **50**, 3625–3647, https://doi.org/10.1007/s00382-017-3830-7.

Chen, H. M., W. H. Yuan, J. Li, and R. C. Yu, 2012: A possible cause for different diurnal variations of warm season rainfall as shown in station observations and TRMM 3B42 data over the southeastern Tibetan plateau. *Adv. Atmos. Sci.*, **29**, 193–200, https://doi.org/10.1007/s00376-011-0218-1.

Chu, W. C., Y. L. Lin, and M. Zhao, 2022: Implementation and evaluation of a double-plume convective parameterization in NCAR CAM5. *J. Climate*, **35**, 617–637, https://doi.org/10.1175/JCLI-D-21-0267.1.

Collins, W. D., and Coauthors, 2004: Description of the NCAR community atmosphere model (CAM 3.0). NCAR/TN-464+STR, 214 pp.

Covey, C., P. J. Gleckler, C. Doutriaux, D. N. Williams, A. G. Dai, J. Fasullo, K. Trenberth, and A. Berg, 2016: Metrics for the diurnal cycle of precipitation: Toward routine benchmarks for climate models. *J. Climate*, **29**, 4461–4471, https://doi.org/10.1175/JCLI-D-15-0664.1.

Cui, Z. Y., G. J. Zhang, Y. Wang, and S. C. Xie, 2021: Understanding the roles of convective trigger functions in the diurnal cycle of precipitation in the NCAR CAM5. *J. Climate*, **34**, 6473–6489, https://doi.org/10.1175/jcli-d-20-0699.1.

Dai, A. G., 2001: Global precipitation and thunderstorm frequencies. Part II: Diurnal variations. *J. Climate*, **14**, 1112–1128, https://doi.org/10.1175/1520-0442(2001)014<1112:GPATFP>2.0.CO;2.

Dai, A. G., 2006: Precipitation characteristics in eighteen coupled climate models. *J. Climate*, **19**, 4605–4630, https://doi.org/10.1175/JCLI3884.1.

Ding, Y. H., and J. C. L. Chan, 2005: The East Asian summer monsoon: An overview. *Meteorol. Atmos. Phys.*, **89**, 117–142, https://doi.org/10.1007/s00703-005-0125-z.

Eyring, V., and Coauthors, 2021: Human influence on the climate system. *Climate Change 2021: The Physical Science Basis. Contribution of Working Group I to the Sixth Assessment Report of the Intergovernmental Panel on Climate Change,* Masson-Delmotte et al., Eds., Cambridge University Press, Cambridge, United Kingdom and New York, NY, USA, 423–552, doi: 10.1017/9781109157896.005.

Flato, G., and Coauthors, 2013: Evaluation of climate models. In: Climate change 2013: the physical science basis. [Stocker TF, Qin D, Plattner GK, Tignor M, Allen SK, Boschung J, Nauels A, Xia Y, Bex V, Midgley PM (eds)], Cambridge University Press, Cambridge, New York, 741–866.

Gettelman, A., and Coauthors, 2010: Global simulations of ice nucleation and ice supersaturation with an improved cloud scheme in the Community Atmosphere Model. *J. Geophys. Res*, **115**, D18216, https://doi.org/10.1029/2009JD013797.

Hersbach, H., and Coauthors, 2020: The ERA5 global reanalysis. *Quart. J. Roy. Meteor. Soc.*, **146**, 1999–2049, https://doi.org/10.1002/qj.3803.

Huang, D.-Q., J. Zhu, Y.-C. Zhang, and A.-N. Huang, 2013: Uncertainties on the simulated summer precipitation over Eastern China from the CMIP5 models. *J. Geophys. Res.*, **118**, 9035–9047, https://doi.org/10.1002/jgrd.50695.

Huffman, G., D. Bolvin, D. Braithwaite, K. Hsu, and R. Joyce, 2018: Algorithm theoretical basis document (ATBD) NASA global precipitation measurement (GPM) integrated Multi-satellitE retrievals for GPM (IMERG). NASA, 29 pp.

Iacono, M. J., J. S. Delamere, E. J. Mlawer, M. W. Shephard, S. A. Clough, and W. D. Collins, 2008: Radiative forcing by long-lived greenhouse gases: Calculations with the AER radiative transfer models. *J. Geophys. Res.*, **113**, D13103, https://doi.org/10.1029/2008JD009944.

Kain, J. S., 2004: The Kain - Fritsch convective parameterization: An update. *J. Appl. Meteorol.*, **43**, 170–181, https://doi.org/10.1175/1520-0450(2004)043<0170:TKCPAU>2.0.CO;2.

Li, J., R. C. Yu, W. H. Yuan, H. M. Chen, W. Sun, and Y. Zhang, 2015: Precipitation over East Asia simulated by NCAR CAM5 at different horizontal resolutions. *Journal of Advances in Modeling Earth Systems*, **7**, 774–790, https://doi.org/10.1002/2014MS000414.

Li, J. H., and Y. Zhang, 2022: Enhancing the stability of a global model by using an adaptively implicit vertical moist transport scheme. *Meteorol. Atmos. Phys.*, **134**, 55, https://doi.org/10.1007/s00703-022-00895-5.

Li, X. H., Y. Zhang, X. D. Peng, and J. Li, 2020: Using a single column model (SGRIST1.0) for connecting model physics and dynamics in the Global-to-Regional Integrated forecast SysTem (GRIST-A20.8). *Geoscientific Model Development Discussions*, in press, https://doi.org/10.5194/gmd-2020-254.

Li, X. H., Y. Zhang, X. D. Peng, W. C. Chu, Y. L. Lin, and J. Li, 2022: Improved climate simulation by using a double-plume convection scheme in a global model. *J. Geophys. Res.*, **127**, e2021JD036069, https://doi.org/10.1029/2021JD036069.

Lin, C. G., D. L. Chen, K. Yang, and T. H. Ou, 2018: Impact of model resolution on simulating the water vapor transport through the central Himalayas: Implication for models' wet bias over the Tibetan Plateau. *Climate Dyn.*, **51**, 3195–3207, https://doi.org/10.1007/s00382-018-4074-x.

Lin, L., A. Gettelman, Y. Y. Xu, C. L. Wu, Z. L. Wang, N. Rosen-

bloom, S. C. Bates, and W. J. Dong, 2019: CAM6 simulation of mean and extreme precipitation over Asia: Sensitivity to upgraded physical parameterizations and higher horizontal resolution. *Geoscientific Model Development*, **12**, 3773–3793, https://doi.org/10.5194/gmd-12-3773-2019.

Liu, Z., Y. Zhang, X. M. Huang, J. Li, D. Wang, M. Q. Wang, and X. Huang, 2020: Development and performance optimization of a parallel computing infrastructure for an unstructured-mesh modelling framework. *Geoscientific Model Development Discussions*, in press, https://doi.org/10.5194/gmd-2020-158.

Muetzelfeldt, M. R., R. Schiemann, A. G. Turner, N. P. Klingaman, P. L. Vidale, and M. J. Roberts, 2021: Evaluation of Asian summer precipitation in different configurations of a high-resolution general circulation model in a range of decision-relevant spatial scales. *Hydrology and Earth System Sciences*, **25**, 6381–6405, https://doi.org/10.5194/hess-25-6381-2021.

Neale, R. B., J. H. Richter, and M. Jochum, 2008: The impact of convection on ENSO: From a delayed oscillator to a series of events. *Journal of Climate*, **21**(22), 5904–5924, https://doi.org/10.1175/2008JCLI2244.1.

Niu, G.-Y., and Coauthors, 2011: The community Noah land surface model with multiparameterization options (Noah-MP): 1. Model description and evaluation with local-scale measurements. *J. Geophys. Res.*, **116**, D12109, https://doi.org/10.1029/2010JD015139.

Park, S., and C. S. Bretherton, 2009: The university of washington shallow convection and moist turbulence schemes and their impact on climate simulations with the community atmosphere model. *J. Climate*, **22**, 3449–3469, https://doi.org/10.1175/2008JCLI2557.1.

Park, S., C. S. Bretherton, and P. J. Rasch, 2014: Integrating cloud processes in the community atmosphere model, version 5. *J. Climate*, **27**, 6821–6856, https://doi.org/10.1175/JCLI-D-14-00087.1.

Rio, C., A. D. Del Genio, and F. Hourdin, 2019: Ongoing breakthroughs in convective parameterization. *Current Climate Change Reports*, **5**, 95–111, https://doi.org/10.1007/s40641-019-00127-w.

Song, F. F., and G. J. Zhang, 2017: Improving trigger functions for convective parameterization schemes using GOAmazon observations. *J. Climate*, **30**, 8711–8726, https://doi.org/10.1175/JCLI-D-17-0042.1.

Tang, Q., and Coauthors, 2019: Regionally refined test bed in E3SM atmosphere model version 1 (EAMv1) and applications for high-resolution modeling. *Geoscientific Model Development*, **12**, 2679–2706, https://doi.org/10.5194/gmd-12-2679-2019.

Tang, S. Q., P. Gleckler, S. C. Xie, J. Lee, M.-S. Ahn, C. Covey, and C. Z. Zhang, 2021: Evaluating the diurnal and semidiurnal cycle of precipitation in CMIP6 models using satellite- and ground-based observations. *J. Climate*, **34**, 3189–3210, https://doi.org/10.1175/jcli-d-20-0639.1.

Taylor, K. E., D. L. Williamson, and F. Zwiers, 2000: The sea surface temperature and sea-ice concentration boundary conditions for AMIP II simulations. PCMDI Report No. 60, 25 pp.

Wang, J. Y., and D. A. Randall, 1994: The moist available energy of a conditionally unstable atmosphere. Part II: Further analysis of GATE data. *J. Atmos. Sci.*, **51**, 703–710, https://doi.org/10.1175/1520-0469(1994)051<0703:TMAEOA>2.0.CO;2.

Wang, L., Y. Zhang, J. Li, Z. Liu, and Y. H. Zhou, 2019: Understanding the performance of an unstructured-mesh global shallow water model on kinetic energy spectra and nonlinear vorticity dynamics. *Journal of Meteorological Research*, **33**, 1075–1097, https://doi.org/10.1007/s13351-019-9004-2.

Wang, Y., G. J. Zhang, and Y. Q. Jiang, 2018: Linking stochasticity of convection to large-scale vertical velocity to improve Indian Summer Monsoon simulation in the NCAR CAM5. *J. Climate*, **31**, 6985–7002, https://doi.org/10.1175/JCLI-D-17-0785.1.

Wu, T. W., and Coauthors, 2019: The Beijing climate center climate system model (BCC-CSM): The main progress from CMIP5 to CMIP6. *Geoscientific Model Development*, **12**, 1573–1600, https://doi.org/10.5194/gmd-12-1573-2019.

Xie, S. C., and M. H. Zhang, 2000: Impact of the convection triggering function on single-column model simulations. *J. Geophys. Res.*, **105**, 14 983–14 996, https://doi.org/10.1029/2000JD900170.

Xie, S. C., and Coauthors, 2019: Improved diurnal cycle of precipitation in E3SM with a revised convective triggering function. *Journal of Advanceds Modeling Earth Systems*, **11**, 2290–2310, https://doi.org/10.1029/2019MS001702.

Xin, X. G., T. W. Wu, J. Zhang, J. C. Yao, and Y. J. Fang, 2020: Comparison of CMIP6 and CMIP5 simulations of precipitation in China and the East Asian summer monsoon. *International Journal of Climatology*, **40**, 6423–6440, https://doi.org/10.1002/joc.6590.

Yang, G.-Y., and J. Slingo, 2001: The diurnal cycle in the tropics. *Mon. Wea. Rev.*, **129**, 784–801, https://doi.org/10.1175/1520-0493(2001)129<0784:TDCITT>2.0.CO;2.

Yu, R. C., T. J. Zhou, A. Y. Xiong, Y. J. Zhu, and J. M. Li, 2007: Diurnal variations of summer precipitation over contiguous China. *Geophys. Res. Lett.*, **34**, L01704, https://doi.org/10.1029/2006GL028129.

Yu, R. C., J. Li, Y. Zhang, and H. M. Chen, 2015: Improvement of rainfall simulation on the steep edge of the Tibetan Plateau by using a finite-difference transport scheme in CAM5. *Climate Dyn.*, **45**, 2937–2948, https://doi.org/10.1007/s00382-015-2515-3.

Yuan, W. H., R. C. Yu, M. H. Zhang, W. Y. Lin, J. Li, and Y. F. Fu, 2013: Diurnal cycle of summer precipitation over subtropical East Asia in CAM5. *J. Climate*, **26**, 3159–3172, https://doi.org/10.1175/JCLI-D-12-00119.1.

Zhang, G. J., 2002: Convective quasi-equilibrium in midlatitude continental environment and its effect on convective parameterization. *J. Geophys. Res.*, **107**, 4220, https://doi.org/10.1029/2001JD001005.

Zhang, G. J., and N. A. McFarlane, 1995: Sensitivity of climate simulations to the parameterization of cumulus convection in the canadian climate centre general circulation model. *Atmosphere-Ocean*, **33**, 407–446, https://doi.org/10.1080/07055900.1995.9649539.

Zhang, Y., and H. M. Chen, 2016: Comparing CAM5 and superparameterized CAM5 simulations of summer precipitation characteristics over continental East Asia: Mean state, frequency-intensity relationship, diurnal cycle, and influencing factors. *J. Climate*, **29**, 1067–1089, https://doi.org/10.1175/JCLI-D-15-0342.1.

Zhang, Y., and J. Li, 2016: Impact of moisture divergence on systematic errors in precipitation around the Tibetan Plateau in a general circulation model. *Climate Dyn.*, **47**, 2923–2934,

https://doi.org/10.1007/s00382-016-3005-y.

Zhang, Y., J. Li, R. C. Yu, S. X. Zhang, Z. Liu, J. H. Huang, and Y. H. Zhou, 2019: A layer-averaged nonhydrostatic dynamical framework on an unstructured mesh for global and regional atmospheric modeling: Model description, baseline evaluation, and sensitivity exploration. *Journal of Advances in Modeling Earth Systems*, **11**, 1685–1714, https://doi.org/10.1029/2018MS001539.

Zhang, Y., J. Li, R. C. Yu, Z. Liu, Y. H. Zhou, X. H. Li, and X. M. Huang, 2020: A multiscale dynamical model in a dry-mass coordinate for weather and climate modeling: Moist dynamics and its coupling to physics. *Monthly Weather Review*, **148**, 2671–2699, https://doi.org/10.1175/MWR-D-19-0305.1.

Zhang, Y., R. C. Yu, J. Li, X. H. Li, X. Y. Rong, X. D. Peng, and Y. H. Zhou, 2021: AMIP simulations of a global model for unified weather-climate forecast: Understanding precipitation characteristics and sensitivity over East Asia. *Journal of Advanceds in Modeling Earth Systems*, **13**, e2021MS002592, https://doi.org/10.1029/2021ms002592.

Zhang, Y., X. H. Li, Z. Liu, X. Y. Rong, J. Li, Y. H. Zhou, and S. Y. Chen, 2022: Resolution sensitivity of the GRIST nonhydrostatic model from 120 to 5 km (3.75 km) during the DYAMOND winter. *Earth and Space Science*, **9**, e2022EA002401, https://doi.org/10.1029/2022EA002401.

Zhang, Y. Y., and S. A. Klein, 2010: Mechanisms affecting the transition from shallow to deep convection over land: inferences from observations of the diurnal cycle collected at the ARM southern great plains site. *Journal of the Atmospheric Sciences*, **67**, 2943–2959, https://doi.org/10.1175/2010JAS3366.1.

Zhou, Y. H., Y. Zhang, J. Li, R. C. Yu, and Z. Liu, 2020: Configuration and evaluation of a global unstructured mesh atmospheric model (GRIST-A20.9) based on the variable-resolution approach. *Geoscientific Model Development*, **13**, 6325–6348, https://doi.org/10.5194/gmd-13-6325-2020.